Available online at www.sciencedirect.com
ScienceDirect
Journal of Colloid and Interface Science 302 (2006) 633–642
JOURNAL OF Colloid and Interface Science
www.elsevier.com/locate/jcis

Structural variations in a family of orthodialkoxyarenes organogelators

Pierre Terech [a,*], Gilles Clavier [b], Henri Bouas-Laurent [b], Jean-Pierre Desvergne [b], Bruno Demé [c], Jean-Luc Pozzo [b]

[a] *UMR 5819 CEA-CNRS–Univ. J. Fourier, DRFMC-SI3M, CEA-Grenoble 17, rue des Martyrs, 38054 Grenoble Cedex 9, France*
[b] *Laboratoire de Chimie Organique et Organométallique, LCOO, UMR 5802 CNRS, Université Bordeaux 1, 351, Cours de la Libération, 33405 Talence, France*
[c] *Institut Laue Langevin, 6 rue Jules Horowitz, BP 156, 38042 Grenoble Cedex 9, France*

Received 1 March 2006; accepted 29 June 2006

Available online 4 July 2006

Abstract

A series of low mass organic gelators (LMOGS) **1** to **6** whose chemical structures have in common an orthodialkoxyarene feature was prepared in order to compare the shape of their fibrillar network as investigated by small-angle neutron scattering (SANS) experiments. All members of the family exhibit a pronounced tendency to bundle formation by merging isolated fibers in extended packets of average diameter >500 Å. Variations of the 2D packing symmetry are observed from hexagonal to square orderings with close derivatives of the reference member 2,3-didecyloxyanthracene (DDOA). Networks in which the fraction of isolated fibers is significant enough to allow for their SANS identification are those for 6,7-dichloro-2,3-didecyloxyanthracene (Cl_2DDOA) and 2,3-dodecyloxy-9,10-anthraquinone (**5**). For this latter, the monodispersity of the cross-sections (thickness = 74 Å) is remarkable and the rectangular shape ($b/a \sim 0.12$) accounts for a merging mechanism into anisotropic bundles (ribbons).

Keywords: Gel; Neutron scattering; Structures; Network; Fiber; Bundles

1. Introduction

Molecular gels are innovative materials in the field of thermoreversible gels. The emergent [1–6] domain of research in soft condensed matter takes advantage of the spontaneous self-assembling phenomenon to form giant meshes of fibers from small molecules ($M_W \leqslant 1000$) [7–19]. The cohesive energies characteristic of the fibers and their nodal zones in the gel networks are of the order of the thermal energy accounting for the remarkable reversibility between the sol and gel states and the associated structures and properties involved at various scales. Water [20] or organic liquids [1] and mixtures can be gelated by specialist molecules part of an increasing large library. Frequently, low molecular mass organic gelators (LMOGs) [21] bear hydroxyl groups useful to develop electrostatic interactions (hydrogen bonds) generating the linear assemblies. Here, we focus on a subclass of aromatic compounds, 2,3-di-*n*-alkoxyanthracenes (**1**, Scheme 1) without such hydroxyl groups and shown [12,22–25] to gelate apolar hydrocarbons, alcohols, nitriles, amides, etc. Despite some interesting attempts using molecular modeling [11], the design of LMOGs remains largely empirical due to a subtle solvent-LMOG affinity parameter and the analysis of experimental investigations remains a privileged approach.

The objective of the present study is to design new gelators related to compounds **1** (especially DDOA) through structural modifications of the aromatic part and of the chain length but not of the nature and number (two alkoxy groups) nor the mutual position (ortho substituted along the molecular long axis) of the substituents. Previous experiments have shown that the gel-forming ability of DDOA is also present in benzene derivatives [12] (but **2** is less efficient than **3**) or in 2,3-dihexadecyloxynaphthalene (**4**), or by replacing, in a symmetrical way, the "CH" groups of the middle ring (in compounds **1**) by two "C=O" (**5**) [24] or "N" (**6**) [25], respectively. The new syntheses are conducted so as to maintain or increase the dipole–dipole interactions. Structural consequences of these

* Corresponding author.
E-mail address: pierre.terech@cea.fr (P. Terech).

0021-9797/$ – see front matter
doi:10.1016/j.jcis.2006.06.056

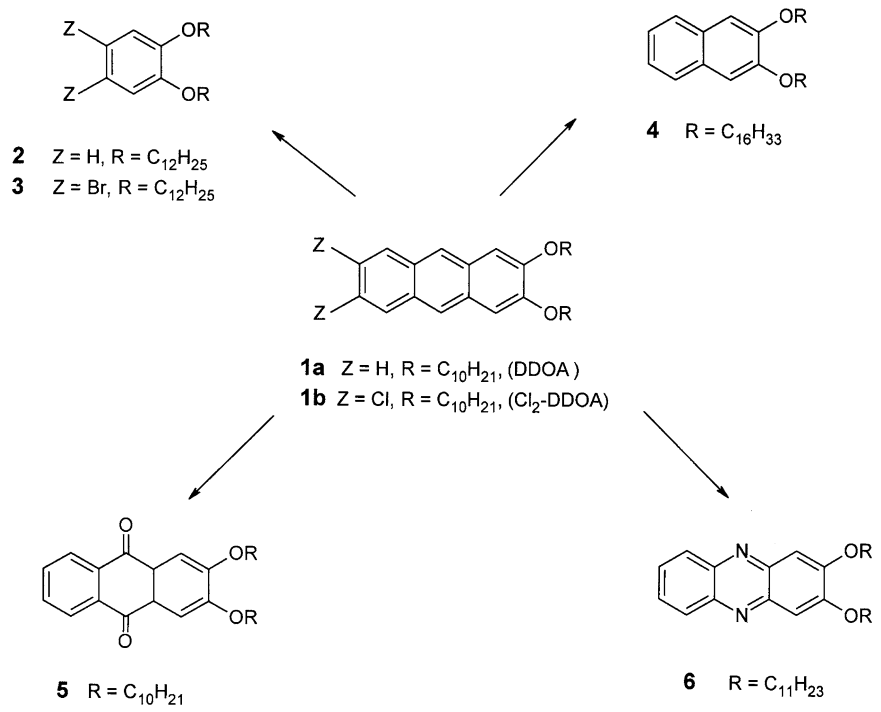

Scheme 1. Investigated family of aromatic gelators structurally related to **1** by modification of the cyclic skeleton in a symmetrical fashion.

molecular modifications on the supramolecular aggregates of the gels are expected. Using the small angle neutron scattering (SANS) technique, we report on the structural features of gels formed with compounds **3**, **4**, **5**, and **6** selected for their optimal stability at ambient temperature.

2. Experimental

Melting temperatures were determined in capillary tubes of a Buchi 510 apparatus. FTIR spectra were recorded on a Perkin Elmer Paragon 1000 spectrophotometer. ^{1}H and ^{13}C NMR spectra used a Bruker 250 AC instrument for solutions in $CDCl_3$ unless stated otherwise. Chemical shifts are in ppm and J values are in Hz. Chromatography separations were performed on SDS Silica Chromagel (70–210 μm). Mass spectra were obtained on an AutoSpeq EQ spectrometer. Elemental analyses were performed by the Microanalytical Service, Institut du Pin, University Bordeaux 1. Electronic absorption spectra and transmission spectra were measured on a Hitachi U-3300 spectrophotometer equipped with a thermo-controlled cell (10 mm optical path-length). For TEM measurements, gels were deposited on formvar coated copper grids in thin slices prepared by ultracryomicrotomy. A carbon coating preceded the examination (JEOL 2000 apparatus).

Gelation tests used the inverted test tube method [4]. The gel-to-sol phase transition temperatures T_m (see Appendix A) were determined using an inverted septum-capped glass tube immersed in a thermo-controlled bath, the temperature being raised at 2 °C min^{-1}. The reported values are the average of several measurements (reproducibility ±1 °C). Details of the syntheses of **3**, **5**, and **6** are given in Appendix A. Alteration of the structures developed in the gels by the isotopic composition of the systems was assumed to be inexistent considering the variety of organic liquids that can be gelled (see Appendix A) and the absence of previous similar observations in the class of low-mass organogels. The gelators were purified and dried (Appendix A), deuterated ethanol and acetonitrile were high quality grades so that the role that might be played by trace amounts of water on the structures was assumed negligible.

Small angle neutron scattering (SANS) measurements were performed using the D11 diffractometer at the Institut Laue Langevin (ILL, Grenoble, France) [26]. Deuterated organic solvents were used (Aldrich) to restrict the level of incoherent scattering of the gels to the contribution of the gelator molecules themselves. The sample–detector distances and neutron wavelengths were adjusted to deliver a scattered wave vector Q-range 0.002 Å^{-1} < Q < 0.25 Å^{-1} ($Q = 4\pi/\lambda \sin\theta$, λ being the neutron wavelength and θ half the scattering angle). Standard corrections and calibration procedures have been used to precede with the radial averaging of isotropic 2D arrays of neutron counts collected on the detector. The level of incoherent background (mainly due to the presence of H atoms of the gelators) to be subtracted from the scattered intensity, was adjusted from a IQ^4 versus Q plot assuming sharp interfaces of the fibrillar aggregates. Intensities represented in all figures are expressed in cm^{-1}. Detailed and rigorous formalisms and protocols concerning the use of the SANS technique for such self-assembled systems are presented elsewhere [27] and references cited therein.

3. Results and analysis

The electron micrograph of Fig. 1 shows that the solid-like part of the gel network for the **4**/ethanol system is made up of

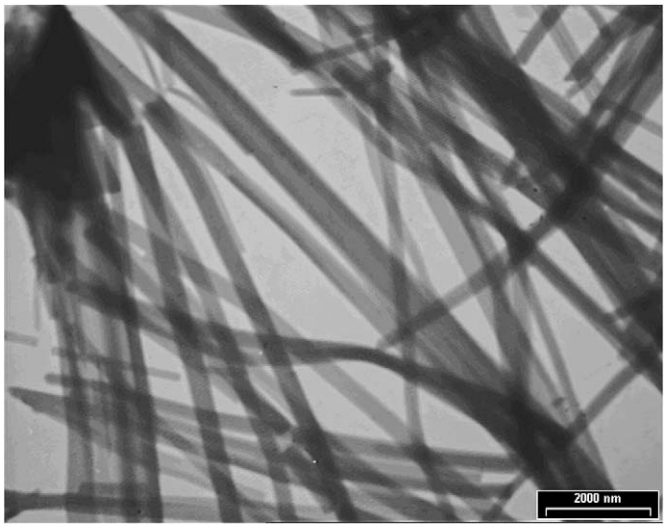

Fig. 1. Transmission electron micrograph showing the filamentary nature of the gel network of 2,3-di-*n*-hexadecyloxynaphthalene (**4**) prepared in ethanol ($C = 2 \times 10^{-2}$ M).

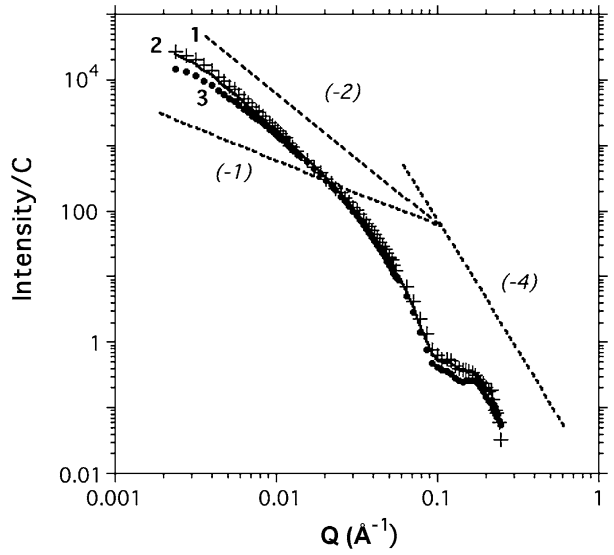

Fig. 2. Concentration normalized small-angle neutron scattering intensity versus Q for **5**/*d*-ethanol organogels. 1 (+): $C = 0.034$ wt%; 2 (—): $C = 0.043$ wt%; 3 (●): $C = 0.100$ wt%. Dotted lines are guides for Q^{-1}, Q^{-2}, Q^{-4} intensity decays.

elongated species. Under the present experimental conditions, fiber-like or ribbon-like 1D species with a range of 200–700 nm diameters are observed. SANS studies of the swollen gels are used to further characterize in the nanoscale the 1D aggregates present in the swollen gel.

3.1. *5* organogels

Fig. 2 shows a selection of concentration-normalized scattering curves for gels of **5** in *d*-ethanol. The profiles are almost superimposable over the whole Q-range indicating that no significant contribution from heterogeneities or nodal zones can be discerned as the concentration is increased [27]. As a result, the scattered intensities can be analyzed in terms of form-

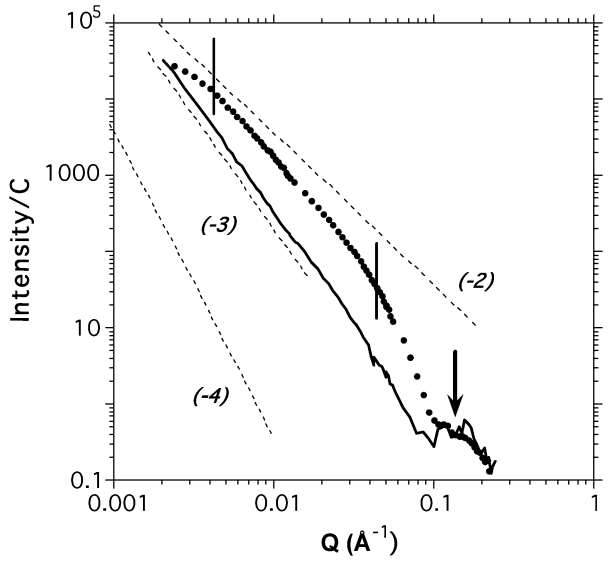

Fig. 3. Concentration normalized SANS intensity versus Q for **5**/*d*-ethanol organogels (●: $C = 0.034$ wt%) and in a 50:50 H/D ethanol mixture (full line: $C = 0.031$ wt%). Guidelines for Q^{-2}, Q^{-3}, Q^{-4} intensity decays are shown as straight segments. The bold arrow points to an oscillation at $Q \sim 0.116$ Å^{-1}. Two vertical bars delineate the scattering features typical of ribbon-like structures (see the text).

factor contributions in a single particle scattering context [28]. Conversely, Fig. 3 shows that the profile and the amplitude of the scattered intensity depend upon the isotopic composition of the solvent. The volumic contrast $\Delta\rho$ for **5** aggregates varies from $\Delta\rho = -4.6397 \times 10^{10}$ cm/cm^3 in the fully deuterated solvent to $\Delta\rho = -1.6092 \times 10^{10}$ cm/cm^3 in the 50/50 CH_3CH_2OH/CD_3CD_2OD mixture. The decrease of the average amplitude of the scattering signal apparently suggests that some aggregates or parts of aggregates in the gel have their scattering contribution partly extinguished in the solvent mixture. The remaining signal has a profile different from the original one as well as the slopes of the intensity decays at low-Q (-2 and -3 respectively for the original signal and the contrast-varied one). These observations compel us to consider the homogeneity of the neutron contrast of **5** aggregates in the gels. In particular, at the Q-resolution and Q-range of the experiment, the neutron contrast can vary along the radial dimensions of the 1D aggregates. The heterogeneous profile of $\Delta\rho$ affects the scattering signal through the radius of gyration of the scatterer (second moment of $\Delta\rho$),

$$\lim I(Q) = (\Delta\rho)^2 \frac{2\pi}{Q^4} S, \quad Q \to \infty, \tag{1}$$

where S is the total interface of the scatterer [28].

In this respect, a first possibility is that the fibers or a second component in the network exhibit a structure allowing a partial contrast matching when the isotopic composition of the solvent is varied. In perdeuterated ethanol, the ca. -2 exponent of the low-Q intensity decay and the flattening observed at $Q \to 0$, reveal that ribbon-like structures [29] form a major component of the **5** SAFINs. The sharper decay at $Q > 0.03$ Å^{-1} and an oscillation at $Q \sim 0.116$ Å^{-1} (secondary maximum) characterize finite and well-defined cross-sections. The evolution to

a Q^{-3} decay is intriguing and might be reminiscent with the limit at large Q-values of $I(Q)$ as in expression (1) for large scatterers with sharp interfaces characterized by a Q^{-4} decay. The SAFIN can be modeled with a two-population system for which the ribbon-like fibrillar component (i.e., ca. Q^{-2} low-Q signature) is apparently and partially contrast-matched. Beside, it has also to be kept in mind that systematic deviations from Porod's law (Q^{-4} decay at large Q following expression (1)) are known to be related to structural particularities of the two-phase system [30]. A finite width of the density transition induces negative deviations while density fluctuations of the two phases induce positive fluctuations. The ideal Porod's situation assumes an infinitely sharp density transition from one phase to the other and an electron density invariant within the phase boundaries. These conditions may not be fulfilled in real materials. To illustrate, a slower decay of the asymptotic law can be observed with materials having rough, self-similar surfaces of dimension $2 \leqslant D_s \leqslant 3$ since the intensity will vary then as $Q^{-(6-D_s)}$ [31]. A second possibility to account for the effect of deuterated ethanol is to consider that the prefactor $\Delta\rho A$ of the general expression (2) for the scattered intensity is considerably enhanced in the H/D solvent. Indeed, the square of the contrast is increased by a factor ca. 5.7 while the cross-section A of the 1D nodal component amplifies also the effect for thick bundles. The resulting signal becomes partly overwhelmed by the interfacial scattering signature of large bundles (assuming an identical contrast for fibers and bundles). This option reasonably avoids contrast arguments of the first option that would contradict the crystalline nature of the DDOA fibers with no solvent inclusions as previously shown [32].

$$I(Q) \propto L\frac{\pi}{Q}\Delta\rho^2 A\psi_c, \tag{2}$$

L being the length of the 1D species of cross-section A, ψ_c being a normalized function describing the cross-sectional scattering component. Three types of cross-sectional shapes of the fibers are considered. First, long ($L/2R > 10$) and rigid fibers present at a volume fraction ϕ in the gel system, generate a scattered intensity with a cross-sectional term involving a Bessel function J_1 of the first kind as in expression:

$$I(Q) = \frac{\phi R^2 \Delta\rho^2}{2Q}\left[\frac{J_1(QR)}{QR}\right]^2. \tag{3}$$

The extreme situation of aggregates with very anisotropic cross-sections as probed by SANS (in the experimental Q_{min} limit) is considered with expression (4). t is the thickness of the very flat ribbons with $2a$ being the long side of the cross-sections such that $A = 2ta$ and $\pi/a \ll Q_{min}$.

$$I(Q) = A\frac{2\pi}{Q^2}(\Delta\rho)^2 t^2\left(\frac{\sin(Qt/2)}{Qt/2}\right)^2. \tag{4}$$

The intermediate situation of ribbons with moderately anisotropic cross-sections is analyzed with expression (5) [33–35] where a, b are respectively half the small and long sides of the cross-sections and the cross-sectional anisometry defined by $\kappa = b/a$.

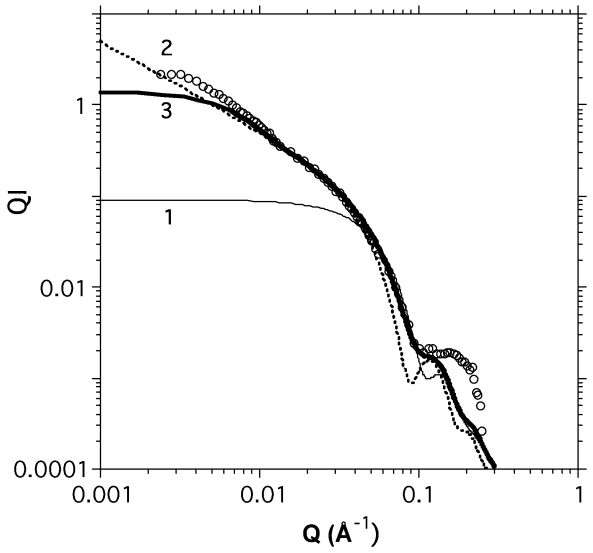

Fig. 4. SANS of a **5**/*d*-ethanol organogel ($C = 0.034$ wt%). Theoretical profiles for: 1 (full line), cylindrical fibers ($R = 40$ Å) according to expression (3); 2 (dotted line), lamellar scatterers ($t = 74$ Å) according to expression (4); 3 is the theoretical scattering for ribbon-like fibers (full bold line, $b = 37$ Å, $\kappa = b/a = 0.12$) according to expression (5).

$$QI(Q) \propto \int_0^{\pi}\left[\frac{2J_1\left(Qa\sqrt{\left(\frac{1+\kappa^2}{2}\right)+\left(\frac{1-\kappa^2}{2}\right)\cos\varphi}\right)}{Qa\sqrt{\left(\frac{1+\kappa^2}{2}\right)+\left(\frac{1-\kappa^2}{2}\right)}}\right]^2 d\varphi. \tag{5}$$

Fig. 4 (curves 1, 2) shows two of the simplest solutions to analyze the experimental profile in a QI versus Q representation for organogels in perdeuterated ethanol. The theoretical scattering curves for cylindrical fibers (Q^{-1} asymptotic decay at low-Q) and lamellar aggregates (Q^{-2} asymptotic decay at low-Q) have been appropriately chosen to show up a similar oscillation at $Q \sim 0.116$ Å^{-1}. It follows that discrepancies on the remaining Q-range of the scattering curves suggest that, on the length scale corresponding to the Q-range investigated, the aggregates appear more like lamellar species. Considering that **4** SAFINs in ethanol molecular gels are made up of fibrillar aggregates, as shown by the TEM view of Fig. 1, it is expected that the cross-sections of the 1D species be anisotropic (ribbon-like fibers). Three scattering features (from low to large Q-values) can be used as guidelines for the analysis: (i) the innermost relative flattening of the profile ($Q < 0.004$ Å^{-1}) associated to a small bump at $Q \sim 0.011$ Å^{-1}, (ii) the power law decay $I \sim Q^{-2.3}$ in the range $0.004 \leqslant Q \leqslant 0.03$ Å^{-1} and (iii) the oscillation at $Q \sim 0.116$ Å^{-1} preceded by a sharper decay. They are characteristic of 1D aggregates with finite sized sections at the origin of the mentioned sharper decay at $Q \sim 0.06$ Å^{-1}. Fig. 4 (curve 3) reproduces these features for long fibers with elliptical (or rectangular) sections. The well-resolved oscillation reveals the monodispersity of the thickness of the ribbon-like fibers. The limited spatial extension of the long axis of the sections is characterized by the kick at $Q \sim 0.004$ Å^{-1}. The corresponding real-space distance agrees with that used for the fit of the scattering profile ($b = 37$ Å). Usually, the nodal zones are bundles where fibers are merging according to

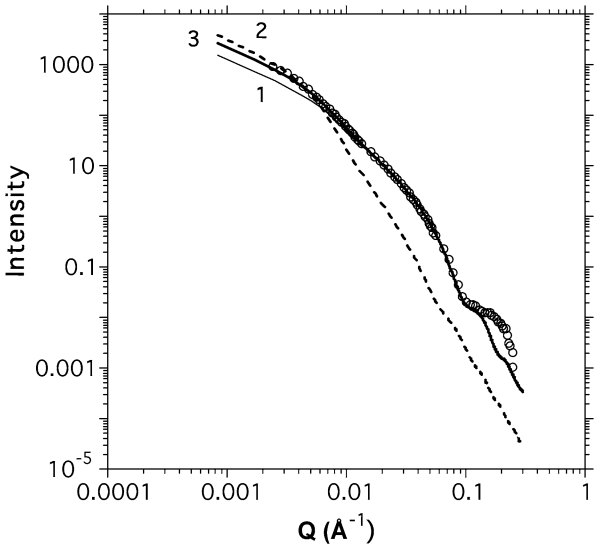

Fig. 5. SANS of a **5**/*d*-ethanol organogel ($C = 0.034$ wt%). The scattered intensity for the two structural components of the network are shown: 1, ribbon-like aggregates with elliptical sections, $\kappa = b/a = 0.12$, $a = 308$ Å; 2, radially polydisperse cylindrical bundles, $R = 450$ Å; 3, 1 + 2 resulting signal.

variable topological mechanisms. Such connection modes define 3D opened pores with fibrillar boundaries that entrap the bulk volume through interfacial capillary forces. The schematic structural description as a two-population system, fibers and bundles, is consistent with the global scattering profile as modeled in Fig. 5. The two scattering components are represented and the resulting intensity describes well all parts of the experimental curve. The average diameter of the bundles (ca. 900 Å) chosen for such agreement is also consistent with that found for other members of the family of orthodialkoxyarenes (vide infra).

The transverse dimension can also be extracted from a $\ln(Q^{\alpha} I)$ versus Q^2 plot as shown in Fig. 6A. The best linear fit is obtained for $\alpha = 2$, as expected with ribbon-like aggregates (no such clear situation is obtained for $\alpha = 1$ typical of cylindrical fibers). The size $t \sim 74.6$ Å is extracted from the slope of the specific plots (see caption, Fig. 6) and the value compares well with that obtained from the fit of the global scattering curve. The linear part is preceded at $Q \to 0$ by a bump whose apex at $Q^* \sim 0.004$ Å^{-1} is a manifestation of the presence of thicker aggregates in the system according to the analysis of Fig. 5. Fig. 6B confirms that the theoretical modeling of the composite signal (ribbons and bundles) reproduces the peak at Q^*. A noticeable scattering difference among the series of orthodialkoxyarenes LMOGs is the absence of Bragg peaks at large Q-values in the experimental Q-range investigated. It has been reported [1] that these peaks usually characterize the molecular ordering in the fibers and their junction zones. It follows that molecular orderings with typical distances corresponding to bilayered organizations (∼2 × 21 Å, see Table 1) in which the long molecular axis lies in the cross-sectional plane are absent in **5** organogels. The aggregation mechanism involves more probably molecular overlaps optimizing the π–π interactions. Moreover, bundles of the **5** gel network are arranged in a way that does not increase the coherence length of the periodicities since increasing the concentration does not generate or enhance any Bragg peak in the Q-range.

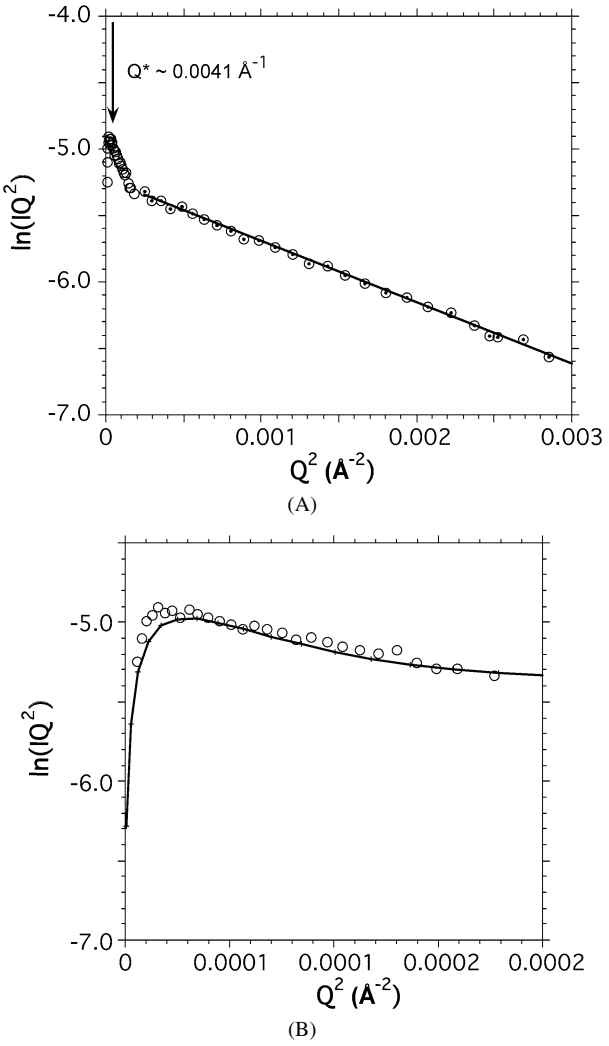

Fig. 6. SANS of a **5**/*d*-ethanol organogel ($C = 0.034$ wt%). Guinier plots for ribbon-like scatterers. (A) From the straight part, the transverse dimension $t = 74$ Å is extracted according to $I(Q) = A(2\pi/Q^2)(\Delta\rho)^2 t^2 \exp -(Q^2 t^2/12)$. The low-$Q$ bump at Q^* is due to the presence of thick bundles (see the text). (B) Enlargement of the $\ln(Q^2 I)$ versus Q^2 plot. (○) Experimental data for $C = 0.034$ wt%; (—) theoretical composite signal of Fig. 5.

3.2. *3 organogels*

The scattering curve for **3** is very different from that of **5** organogels as shown in Fig. 7. A sharp decay ($Q^{-4.2}$) is terminated by a Bragg peak at $Q \sim 0.152$ Å^{-1}. The corresponding reticular distance $\langle d \rangle = 41.3$ Å suggests that overlapped molecules ($l_{\text{mol}} \sim 15$ Å) are involved in the structures. For strongly segregated, randomly interpenetrated phases, the Q^{-4} decay can be theoretically described in a random two-phase model [36]. Here, the description is only approximate and to elucidate the origin of the non-perfect agreement, a Porod's analysis can be conducted in the large-Q range together with a determination of the scattering invariant INV ($\text{INV} = \int_0^{\infty} Q^2 I(Q)\,\mathrm{d}Q = 2\pi^2 V \gamma(0) = (\Delta\rho)^2 \phi(1-\phi) 2\pi^2$). Beside, the final slope at $Q \to \infty$ of the scattering function of

Table 1
Summary of structural features of orthodialkoxyarenes LMOGs and their gel networks

LMOG	Molecular lengths (Å)	Isolated fibers	Bundles
1a DDOA	25/12	No SANS observation	Crystalline 100–500 Å diameter Hexagonal 2D symmetry $\langle d\rangle \sim 63$ Å
1b Cl_2DDOA	26/12	Cylinders (1-octanol) $R \sim 120$ Å Ribbons (cyclohexane) $t \sim 140$ Å	Crystalline (1-octanol) >500 Å $\langle d\rangle \sim 62$ Å Amorphous (cyclohexane)
3	24/5	No SANS observation	Crystalline 1100 Å diameter $\langle d\rangle \sim 41.3$ Å
4	30/7	No SANS observation	Crystalline Square 2D symmetry $\langle d\rangle \sim 73.3$ Å
5	25/12	Ribbons $2b = 74$ Å, $2a \sim 700$ Å	Amorphous (random fusion) 900 Å diameter
6	26/12	No SANS observation	Crystalline 900 Å diameter $\langle d\rangle \sim 44.6$ Å

Note. First column indicates the overall molecular length of the gelator molecules in its extended conformation while the second figure corresponds to the π segment (between the oxygen and Z atom, see Scheme 1). $\langle d\rangle$ is the inter-reticular distance extracted from the Bragg peak(s) at Q^* ($\langle d\rangle = 2\pi/Q^*$).

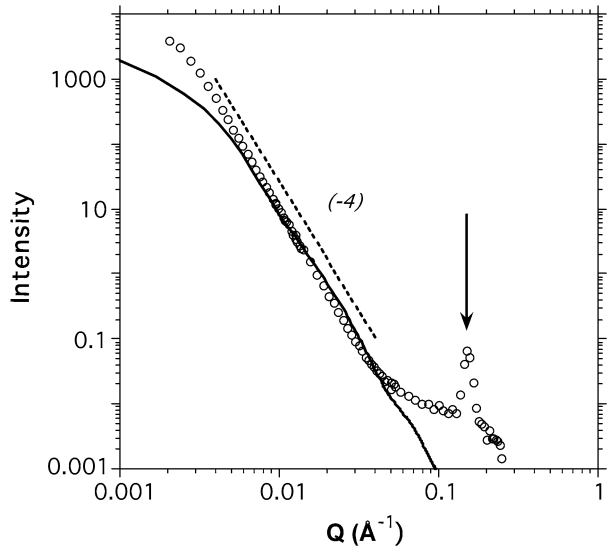

Fig. 7. SANS of a **3**/*d*-acetonitrile organogel (○: $C = 1.09$ wt%). The arrow points to a Bragg peak at $Q \sim 0.152$ Å^{-1}. The straight segment is a guide-line for a Q^{-4} intensity decay. Full line: radially polydisperse ($\Delta R/R \sim 0.22$) cylindrical bundle of fibers ($R = 540$ Å).

any type of scatterer is $\lim I(Q) = (\Delta\rho)^2 \frac{2\pi}{Q^4} S$, S being the total interface of the aggregates. While the extraction of INV and $\lim I(Q)$ require the use of absolute intensities, their combination in the expression $S/V = \pi \lim I(Q) Q^4/\text{INV}$ is independent of any structural model, contrast assumption or calibration of the intensities. To illustrate, a gel of **3** at $C = 1.09$ wt% shows an asymptotic Porod's limit at large Q-values of $\lim(IQ^4) = 7.45 \times 10^{-8}$ cm^{-1} Å^{-4} with INV $= 6.2852 \times 10^{-5}$ cm^{-1} Å^{-3} from which a mean radius value $R \sim 540$ Å can be extracted. Fig. 7 shows the corresponding scattering curve for a form-factor function of cylinders with $R = 540$ Å that correctly reproduces the sharp decay. The sharpness of the Bragg peak indicates that the coherence length over which periodicities of overlapping molecules develop is significant as it can be in a mechanism where fibers merge into bundles. The feature is commonly observed in the class of low-mass organogels [4].

3.3. *4* organogels

4 organogels show a remarkable evolution of the scattering with the gelator concentration. The low-Q decay, close to Q^{-4}, shown in Fig. 8, is typical of large, crystalline aggregates in which molecular periodicities extended over long distances are characterized by large-Q Bragg peaks. Surprisingly, the most concentrated specimen displays a scattering level that is lower than the dilute one despite the concentration normalization procedure. The significant turbidity of the gels shows that large heterogeneities are present and their associated scattering is mainly localized in the angular range limited by the radiation beam stop of the experimental set-up. An additional remarkable scattering feature concerns the sequence and evolution of the Bragg peaks. At low concentration, a series of peaks at 0.0857, 0.126, 0.171 Å^{-1} is identified and corresponds to a 1:1.47:2 sequence. Generally [37], for a rectangular two-dimensional symmetry, i.e., either cmm (centered phase) or pgg (primitive phase) 2D space groups, expression (6) with either $h + k = 2n$ or $h0 = 2n, 0k = 2n$ rules, would define the theoretical sequence for a given b/a ratio.

$$Q_{hk} = 2\pi(h^2 a^{*2} + k^2 b^{*2})^{1/2}. \tag{6}$$

Here, it comes that the ordering of the diffraction centers obeys a square symmetry for which a theoretical sequence $1{:}\sqrt{2}{:}2$ is

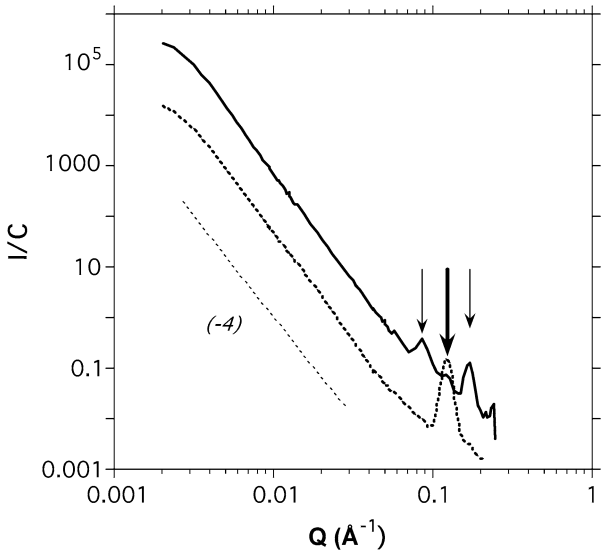

Fig. 8. Concentration normalized SANS curves of **4**/*d*-ethanol organogels. (—) $C = 0.396$ wt%; (···) $C = 5.86$ wt%. The straight segment is a guideline for a Q^{-4} intensity decay. Vertical arrows point to Bragg peaks in a Q-sequence: 0.0857, 0.126, 0.171 Å^{-1}.

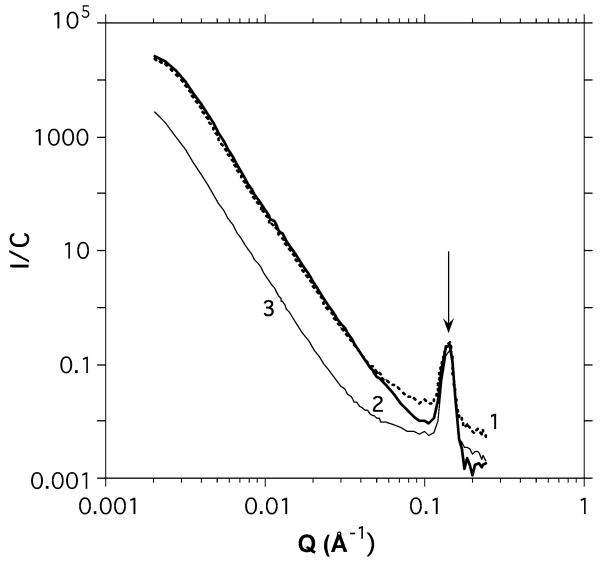

Fig. 9. Concentration normalized curves of **6**/*d*-acetonitrile organogels. 1 (···): $C = 0.589$ wt%; 2 (bold line): $C = 0.833$ wt%; 3 (—): $C = 3.59$ wt%. The arrow points to a Bragg peak at $Q \sim 0.141$ Å^{-1}.

expected. If the concentration is strongly increased, the second peak at 0.123 Å^{-1} overwhelms the signal while the two other peaks vanish. The observation indicates a special mechanism for the formation of the bundle-like heterogeneities. The merging process of the fibers is chemically specific and initiated by the presence of interfacial connection centers that favors the growth of periodicities along determined directions: directions perpendicular to (11) planes generate such anisometric ribbon-like bundles in **4** SAFINs.

3.4. *6* organogels

The typical scattering profile of **6** organogels is a sharp decay followed by a single and intense Bragg peak at $Q = 0.141$ Å^{-1} ($\langle d \rangle \sim 44.6$ Å). The profile is not sensitive to the concentration (Fig. 9) but the sequence of intensity levels does not follow that of concentrations. As for system **3**, it indicates that a significant part of the scattering is hindered by the beam stop: very large heterogeneities are part of the **6** SAFINs. The asymptotic limit at large Q and the estimation of INV are used to extract the average diameter of cylindrical assemblies (ca. 480 ± 30 Å). Beside, the theoretical scattering profile for cylindrical assemblies with $R = 450$ Å reproduces correctly the experimental curve (Fig. 10). A limited departure similar to that observed for **3** gels confirm that the morphology is not unique in the system and that larger aggregates co-exist.

6 can exist in protonated forms (due to the presence of N basic sites on the phenazine moiety, see Scheme 1) in the gel if small amounts of deuterated acid (CF_3COOD) are added in the preparations. Increasing amounts of acid are included in the preparation of the gels at a similar concentration ($C \sim$ 0–5–0.8 wt%, Fig. 11). The shape of the low-Q sharp decay is slightly modified: the flattening startup at very low-Q has almost disappeared. Theoretical simulations of Fig. 11 indicate that an increase of the average diameter to at least ca. 1500 Å is

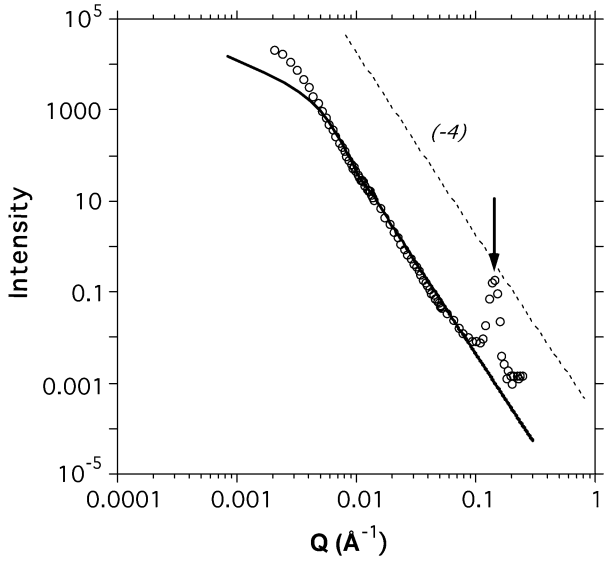

Fig. 10. SANS curve of a **6**/*d*-acetonitrile organogel ($C = 0.833$ wt%). The straight segment is a guideline for a Q^{-4} intensity decay. Full line: radially polydisperse ($\Delta R/R \sim 0.2$) cylindrical bundle of fibers ($R = 450$ Å).

required to produce such an effect. In addition, a slight Q-shift of the Bragg diffraction peak is observed to $Q = 0.136$ Å^{-1} ($\langle d \rangle \sim 46.2$ Å). The packing is slightly looser and produces larger heterogeneities.

4. Conclusion

It is interesting to compare the variety of scattering signatures observed for the various orthodialkoxyarenes with those of close derivatives. Previous scattering measurements [32] have shown that thick bundles of crystalline fibers compose the network of DDOA ($\mu_0 = 1.9$ D) organogels. The diameters of the fibers were in the range 100–500 Å in the swollen gels

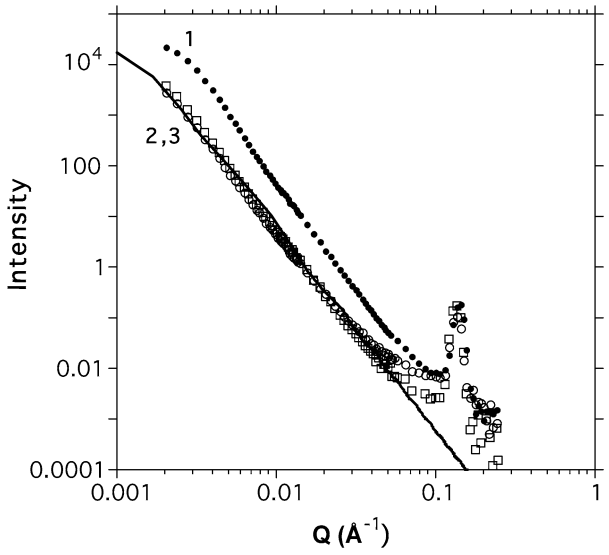

Fig. 11. SANS curves for **6**/*d*-acetonitrile organogels with deuterated perfluoroacetic acid CF_3COOD additions. 1 (●): $C_6 = 0.833$ wt%, $C_{acid} = 0\%$; 2 (□): $C_6 = 0.569$ wt%, $C_{acid} = 3.41$ wt%; 3 (○): $C_6 = 0.518$ wt%, $C_{acid} = 17.04$ wt%. Full line is the theoretical scattering for thick radially polydisperse ($\Delta R/R \sim 0.2$) cylindrical bundles of fibers ($R = 1500$ Å).

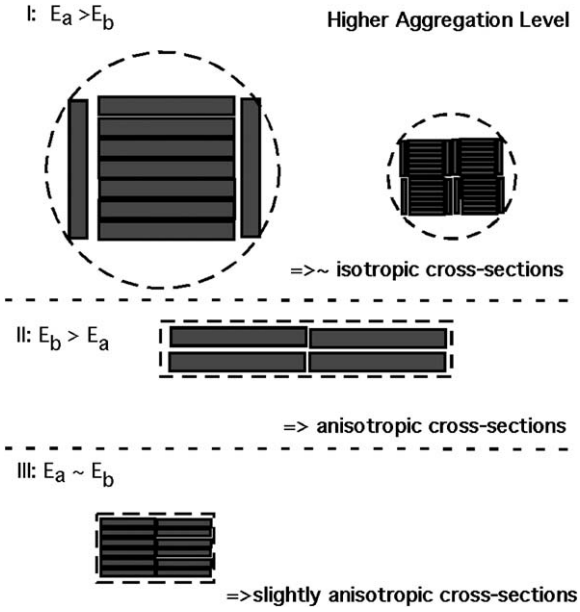

Scheme 2. Schematic drawing of the different options in the bundling process of ribbons according to the relative energy cost due to exposed edges (E_a refers to half the thickness of the ribbon and E_b to half its long side).

while the xerogel exhibited a hexagonal ordering with a reticular periodicity, $\langle d \rangle \sim 63$ Å. Molecular overlaps ($\langle d_{mol} \rangle \sim 24$ Å) are most probably involved in the assemblies of the gel fibers but also in the crystalline states from which the structures in the gels are reminiscent. A 6,7-dichloro derivative Cl_2DDOA was also synthesized and investigated [23] for its fluorescent properties, its higher polarity ($\mu_0 = 3.4$ D) and its ability to form organogels. In this case, thinner fibers ($R \sim 120$ Å) with monodisperse cross-sections form the network in 1-octanol contrasting with the situation for DDOA. In addition, the 1D nanostructures were sensitive to the solvent type from butanol to cyclohexane. Fibers with circular cross-sections ($R \sim 90$ Å) were transformed into tape-like fibers with a thickness $t \sim 140$ Å in cyclohexane. The evolution was pointing at a specific anisotropy of the interfacial polarity of the 1D assemblies. The structural evolution from DDOA to Cl_2DDOA suggests that the increased polarity induces electrostatic effects (due to the separated partial positive and negative charges of the dipoles) that partly counterbalance the long-ranged attractions between the fibers. It appears to be a consequence of a competition between the electrostatics and excluded volume components of the anisotropic potential energy for a semi-dilute system of charged rod-like species [38].

The common feature of this class of organogelators is the high fraction of thick bundles in their networks. These heterogeneities exhibit either a hexagonal or square symmetry (gelators DDOA, Cl_2DDOA or **4**, respectively). The observation of bundles in such self-assembled networks is common and has been confirmed both with transmission electron microscopy [39] and atomic force microscopy experiments [15,40]. Here, the average diameter of the bundles appears to be about 500 Å (with a very large polydispersity) despite the SANS protocol gives access too a much broader range of values. Simple free energy considerations suggest that minimization of the energy cost due to the presence of exposed edges (E_a associated to the long side, E_b associated to the short side) can favor the formation of bundles that associate anisometric cross-sections of isolated fibers to form fagots with more isotropic sections if $E_a \geqslant E_b$. To illustrate, with **5** organogels, the bundling process would involve an aggregation number n of fibers of $n > 12$–15 ribbons (long side $2a \sim 700$ Å) to produce bundles of average diameters 700–850 Å. A second level of aggregation of these fagots would involve ca. 4×12–15 fibers for a resulting overall diameter of the fagot of ca. 1400–1700 Å. Cartoon of Scheme 2 illustrates the naive description. Isolated fibers with monodisperse cross-sections can be observed with Cl_2DDOA and gelator **5**. In both cases, no trivial correlation with the dipolar character can be evoked but an evolution towards anisometric cross-sections is observed with a transverse dimension of the ribbon-like morphologies varying from $t \sim 74$ Å (**5**) to 140 Å (Cl_2DDOA). The protonation of **6** increases significantly the size of the heterogeneities. In conclusion, despite the structural similarities of the five LMOGs, the related self-assembled fibrillar networks propose morphological variations concerning the proportion, size and packing symmetry of the bundles. The packets of bundles can be more or less densely assembled to contribute to the crystallinity of the gels. The associated Bragg diffraction peaks present related real-space distances that are not multiple integers of the molecular lengths. The phenomenology suggests than in the fibers, the gelator molecules are radially shifted (or interdigitated) to maximize the dipolar interactions (π–π) as encountered in various unsaturated π-conjugated systems such as porphyrins [41]. Table 1 summarizes the structural features for the individual gelator molecules, their isolated fibers when present in the gels and their bundles. The consequence of the difference in the dipolar moments on the structures of the aggregates is to favor the formation of thinner and isolated fibers (comparison between

DDOA and Cl_2DDOA). When isolated fibers can be probed by SANS (Cl_2DDOA and **5** gelators) amorphous bundles can be observed. **5** gelator can produce ribbons whose further aggregation modes into bundles can be discussed in terms of interfacial energy cost of the exposed edges. When crystalline-like ordering are observed in the network with high fractions of bundles, the characteristic distances associated to the Bragg peak(s) are not resulting from trivial geometrical relationships with the (partial) molecular lengths. The situation is common for unsaturated and conjugated π systems for which the distinction between two segregative parts in the molecules (as in ordinary surfactants) is more complex and involves molecular offsets and interdigitations.

For future works, it is envisaged to examine the organogels directly in their swollen state either by cryo-transmission electron microscopy protocols [42] or using the environmental scanning electron microscopy (ESEM) technique [43]. ESEM is operating at reduced pressures of solvent vapor (ca. 10 torr) and has shown good resolution imaging (ca. 5 nm for gold-nano-particles) as well as its interest for polymeric based cryogels in the determination of the pore size and thickness in the gel network [44]. The applicability of ESEM to organic liquids will have to be tested as well as the level of beam damage effects (known to be enhanced by the thin liquid layer wetting the specimen under transmission observation).

Acknowledgments

CNRS, Université Bordeaux 1 and "Région Aquitaine" are gratefully acknowledged for financial support. We thank CESAMO for recording the NMR and Mass Spectra, and we are indebted to A. Daléo, C. Martin, V. Massé, and I. Palard for technical assistance. The Institut Laue Langevin is acknowledged for providing access to the neutron beam and all technical assistance.

Appendix A

1,2-dihydroxy-4,5-dibromobenzene was prepared from catechol and bromine as described by van Nostrum et al. [45]. 2,3-dihydroxynaphthalene was of commercial origin. 2,3-dihydroxyphenazine was prepared by refluxing *ortho*-diaminobenzene with 2,5-dihydroxybenzoquinone in ethanol according to Römer et al. [46]. The preparation of **1a** [47], **1b** [23], **2** [12], and **5** [24] were detailed elsewhere. The dialkoxy derivatitves were synthesized by alkylation of *ortho*-diphenols as described in the following general procedure.

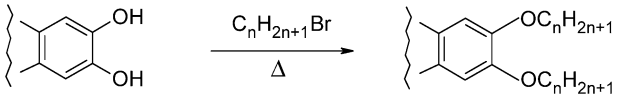

Ortho-diphenol (ca. 10 mmol) and potassium carbonate (2.5 molar equiv. per hydroxy group), dispersed in 2/3 of the solvent (freshly distilled DMF) were introduced in a two-neck round bottom flask equipped with a reflux condenser and a magnetic stirrer and warmed until complete dissolution. The alkylbromide (2.25 molar equiv. per hydroxy group) dissolved in the other part (1/3) of the solvent was quickly added dropwise and refluxed for 12 h. After concentration under reduced pressure, the solid was treated with water and extracted several times with dichloromethane. The organic layers were combined, dried ($MgSO_4$) and then filtered. Subsequent column chromatography on silica, eluted with a mixture of dichloromethane and petroleum ether [v/v: 20/80 (system **A**) or 40/60 (system **B**) or 50/50 (system **C**)] provided the desired product. After concentration, the solid residue was purified by precipitation from an appropriate solvent medium (vide infra).

The preparation of **3**, **4**, and **6** has not been published so far. The relevant elemental analyses and spectroscopic data follow, as well as, some gel melting temperatures T_m.

*4,5-Dibromo-1,2-di-n-dodecyloxybenzene (**3**)* was obtained as white powder (69%); mp 51 °C (from hexane/benzene); Found: C, 63.88; H, 5.64. Calc. for $C_{32}H_{32}O_2Br_2$; C, 63.17; H, 5.30; O, 5.26; Br, 26, 25; [Solvent system **A**]; δ_H (250 MHz) 6.99 (2H, H3 H6); 4.14 (4H, t, $J = 6.5$ Hz, OCH_2); 1.93 (4H, m, OCH_2CH_2); 1.39–1.30 (16H, m, CH_2); 0.93 (6H, t, $J = 6.7$ Hz, CH_3); δ_C (62.9 MHz) 149.1 (C1 and C2); 118.1 (C3 and C6); 114.7 (C4 and C5); 68.7 (OCH_2); 32.0 (d); 29.8 (d); 29.7 (d); 29.5 (d); 29.4 (d, 2C); 29.1 (d); 26.2 (d, 2C); 22.8 (CH_2CH_3); 14.2 (CH_3).

T_m in acetonitrile: 37 °C, 7×10^{-2} M; 30 °C, 4×10^{-2} M; 20 °C, 2.5×10^{-2} M.

*2,3-Di-n-hexadecyloxynaphthalene (**4**)* was obtained as an amorphous colorless powder (62%); mp 67 °C (from hexane/dichloromethane); Found: C, 82.98; H, 11.64. Calc. for $C_{42}H_{72}O_2$, C, 82.83; H, 11.91; O, 5.25; [Solvent system **B**]; δ_H (250 MHz) 7.64 (2H, m, H5 H8); 7.31 (2H, m, H6 H7); 7.03 (2H, s, H1 H4); 4.12 (4H, t, $J = 6.5$ Hz, OCH_2); 1.82 (4H, m, OCH_2CH_2); 1.44 (4H, m, $OCH_2CH_2CH_2$); 1.32–1.16 (48H, m, $CH_2CH_2CH_3$); 0.85 (6H, t, $J = 6.7$ Hz, CH_3); δ_C (62.9 MHz) 149.7, 129.1, 126.4, 123.9, 108.0, 68.9 (OCH_2); 31.7 (d); 30–28.5 (d, nC); 26.3 (d); 25.8 (d); 22.4 (CH_2CH_3); 13.2 (CH_3). FAB^+ m/z: 609.0 (100), 485 (55).

T_m in ethanol: 69 °C, 1.1×10^{-1} M; 60 °C, 6×10^{-2} M; 50 °C, 2.9×10^{-2} M; 32 °C, 2×10^{-2} M; 20 °C, 1.7×10^{-2} M; also forms gels in DMF, pentanol; hydroxyethylmethylacrylate. Not soluble in methanol, propylenecarbonate.

*2,3-Di-n-decyloxyanthraquinone (**5**)*

T_m in ethanol: 34 °C, 1.1×10^{-2} M; 30 °C, 1×10^{-2} M; 20 °C, 0.5×10^{-2} M.

*2,3-Di-n-undecyloxyphenazine (**6**)* was obtained as an amorphous solid (83%); mp 74–75 °C; Found: C, 78.37; H, 10.12. Calc. for $C_{34}H_{52}N_2O_2$, C, 78.41; H, 10.06; N, 5.38; O, 6.14; [Solvent system **C**]; δ_H (250 MHz) 8.13 (m, 2H, H6 H9); 7.76 (m, 2H, H7 H8); 7.35 (s, 2H, H1 H4); 4.23 (4H, t, $J = 6.5$ Hz, OCH_2); 1.97 (m, 4H, OCH_2CH_2); 1.54 (m, 4H, $OCH_2CH_2CH_2$); 1.25 (m, 28H, CH_2); 0.89 (6H, t, $J = 6.7$ Hz, CH_3); δ_C (62.9 MHz) 154.8 (C2 C3); 142.3 (C4a C10a); 142.1 (C5a C9a); 129.2 (C7 C8); 129.1 (C6 C9); 105.9 (C1 C4); 69.6 (OCH_2); 32.3 ($CH_2CH_2CH_3$); 29.8–29.6 (t, 4C); 29.4 (t); 29.1 (OCH_2CH_2); 26.4 ($OCH_2CH_2CH_2$); 23.1 (CH_2CH_3); 14.5 (CH_3). FAB^+ m/z: 521.3 (100), 367.1 (19), 213 (68).

IR: (KBr pellets) 2955, 2915, 2848, 1632, 1571, 1531, 1494, 1469, 1390, 1316, 1227, 1193, 1066, 838, 753, and 593 cm^{-1}.

T_m in acetonitrile: 42 °C, 2×10^{-2} M; 30 °C, 1.6×10^{-2} M; 20 °C, 1.4×10^{-2} M.

References

[1] P. Terech, R.G. Weiss, Chem. Rev. 97 (1997) 3133.
[2] D.J. Abdallah, R.G. Weiss, Adv. Mater. 12 (2000) 1237.
[3] N.M. Sangeetha, U. Maitra, Chem. Soc. Rev. 34 (2005) 821.
[4] R.G. Weiss, P. Terech, Molecular Gels: Materials with Self-Assembled Fibrillar Networks, Springer, Dordrecht, 2006.
[5] P. Terech, Ber. Bunsenges. Phys. Chem. 102 (1998) 1630.
[6] P.S. Russo, in: P.S. Russo (Ed.), Reversible Polymeric Gels and Related Systems, in: Symposium Series, vol. 350, ACS, Washington, DC, 1987, chapter 9.
[7] V. van Esch, S. de Feter, R.M. Kellog, F. de Schryver, B.L. Feringa, Chem. Eur. J. 3 (1997) 1238.
[8] K. Yoza, Y. Ono, K. Yoshihara, T. Akao, H. Shinmori, M. Takeuchi, S. Shinkai, D. Reinhoudt, J. Chem. Soc. Chem. Commun. (1998) 907.
[9] S. Shinkai, K. Murata, J. Mater. Chem. 8 (1998) 485.
[10] U. Maitra, P.V. Kumar, N. Chandra, L.J. D'Souza, M.D. Prasanna, A.R. Raju, J. Chem. Soc. Chem. Commun. (1999) 595.
[11] J. van Esch, F. Schoonbeek, M. de Loos, H. Kooijman, A.L. Spek, R.M. Kellog, B.L. Feringa, Chem. Eur. J. 5 (1999) 937.
[12] G. Clavier, M. Mistry, F. Fages, J.L. Pozzo, Tetrahedron Lett. 40 (1999) 9021.
[13] L.A. Cuccia, J.-M. Lehn, J.-C. Homo, M. Schmutz, Angew. Chem. Int. Ed. 39 (2000) 233.
[14] L. Lu, M. Cocker, R.E. Bachman, R.G. Weiss, Langmuir 16 (2000) 20.
[15] R. Wang, C. Geiger, L. Chen, B. Swanson, D.G. Whitten, J. Am. Chem. Soc. 122 (2000) 2399.
[16] L.N. Lucas, J. van Esch, R.M. Kellog, B.L. Feringa, Chem. Commun. (2001) 759.
[17] A. Ajayaghosh, S.J. George, J. Am. Chem. Soc. 123 (2001) 5148.
[18] M. Koelbel, F.M. Menger, J. Chem. Soc. Chem. Commun. (2001) 275.
[19] M. George, R.G. Weiss, J. Am. Chem. Soc. 123 (2001) 10393.
[20] B. Pfannemüller, W. Welte, Chem. Phys. Lipids 37 (1985) 227.
[21] D.J. Abdallah, R.G. Weiss, Langmuir 16 (2000) 352.
[22] T. Brotin, R. Utermöhlen, F. Fages, H. Bouas-Laurent, J.P. Desvergne, Chem. Soc. Chem. Commun. (1991) 416.
[23] P. Terech, D. Meerschaut, J.-P. Desvergne, M. Colomes, H. Bouas-Laurent, J. Colloid Interface Sci. 261 (2003) 441.
[24] G. Clavier, J.F. Brugger, H. Bouas-Laurent, J.L. Pozzo, J. Chem. Soc. Perkin Trans. 2 (1998) 2527.
[25] J.L. Pozzo, G. Clavier, J.-P. Desvergne, J. Mater. Chem. 8 (1998) 2575.
[26] http://www.ill.fr.
[27] P. Terech, in: R.G. Weiss, P. Terech (Eds.), Molecular Gels: Materials with Self-Assembled Fibrillar Networks, Springer, Dordrecht, 2006, chapter X.
[28] O. Glatter, O. Kratky, Small Angle X-Ray Scattering, Academic Press, London, 1982.
[29] P. Terech, N.M. Sangeetha, B. Deme, U. Maitra, J. Phys. Chem. B 109 (2005) 12270.
[30] W. Ruland, J. Appl. Cryst. 4 (1971) 70.
[31] L. Auvray, P. Auroy, in: P. Lindner, T. Zemb (Eds.), Neutron, X-Ray and Light Scattering, Elsevier, Amsterdam, 1991, pp. 199–221.
[32] P. Terech, J.P. Desvergne, H. Bouas-Laurent, J. Colloid Interface Sci. 174 (1995) 258.
[33] P. Mittelbach, G. Porod, Acta Phys. Austriaca 14 (1961) 185.
[34] J.S. Pedersen, P. Schurtenberger, J. Appl. Cryst. 29 (1996) 646.
[35] J.S. Pedersen, Adv. Colloid Interface Sci. 70 (1997) 171.
[36] P. Debye, A.M. Bueche, J. Appl. Phys. 20 (1949) 518.
[37] S. Hyde, in: K. Holmberg (Ed.), Handbook of Applied Surface and Colloid Chemistry, Wiley, London, 2001, pp. 299–332.
[38] G.A. Carri, M. Muthukumar, J. Chem. Phys. 111 (1999) 1765.
[39] R.H. Wade, P. Terech, E.A. Hewat, R. Ramasseul, F. Volino, J. Colloid Interface Sci. 114 (1986) 442.
[40] B.A. Simmons, C.E. Taylor, F.A. Landis, V.T. John, G.L. McPherson, D.K. Schwartz, R. Moore, J. Am. Chem. Soc. 123 (2001) 2414.
[41] C.A. Hunter, J.K.M. Sanders, J. Am. Chem. Soc. 112 (14) (1990) 5525.
[42] Y. Talmon, in: B.P. Binks (Ed.), Modern Characterization Methods of Surfactant Systems, Dekker, New York, 1999, p. 147.
[43] A. Bogner, G. Thollet, D. Basset, P.H. Jouneau, C. Gauthier, Ultramicroscopy 104 (2005) 290.
[44] F.M. Plieva, M. Karlsson, M.-R. Aguilar, D. Gomez, S. Mikhalovsky, I.Y. Galaev, Soft Matter 1 (2005) 303.
[45] C.F. van Nostrum, S.J. Picken, A.-J. Schouten, R.J.M. Nolte, J. Am. Chem. Soc. 117 (1995) 9957.
[46] A. Romer, H. Budzikiewics, H. Korth, G. Pulverer, Tetrahedron Lett. (1979) 509.
[47] J.-L. Pozzo, G.M. Clavier, M. Colomes, H. Bouas-Laurent, Tetrahedron 53 (1997) 6377.